Ocean Dynamics manuscript No.
(will be inserted by the editor)

A long-term nearshore wave hindcast for Ireland: Atlantic and Irish Sea coasts (1979 - 2012)

Present wave climate and energy resource assessment

Sarah Gallagher · **Roxana Tiron** · **Frédéric Dias**

Received: date / Accepted: date

Abstract The Northeast Atlantic possesses some of the highest wave energy levels in the world. Recent years have witnessed a renewed interest in harnessing this vast energy potential. Due to the complicated geomorphology of the Irish coast, there can be a significant variation in both the wave and wind climate. Long-term hindcasts with high spatial resolution, properly calibrated against available measurements, provide vital information for future deployments of ocean renewable energy installations. These can aid in the selection of adequate locations for potential deployment and for the planning and design of those marine operations. A 34 year (from 1979 to 2012), high-resolution wave hindcast was performed for Ireland including both Atlantic and Irish Sea coasts, with a particular focus on the wave energy resource. The wave climate was estimated using the third generation spectral wave model WAVEWATCH III version 4.11, the unstructured grid formulation. The wave model was forced with directional wave spectral data and 10m winds from the European Centre for Medium Range Weather Forecasts (ECMWF) ERA-Interim reanalysis, which is available from 1979 to the present. The model was validated against available observed satellite altimeter and buoy data, particularly in the nearshore, and was found to be excellent. A strong spatial and seasonal variability was found for both significant wave heights and the wave energy flux, particularly on the north and west coasts. A strong correlation between the NAO teleconnection pattern and wave heights, wave periods and peak direction in winter and also, to a lesser extent, in spring was identified.

Keywords hindcast · wave climate · marine renewable energy · interannual variability · teleconnection patterns · Ireland

S. Gallagher · R. Tiron · F. Dias
UCD School of Mathematical Sciences,
University College Dublin,
Belfield, Dublin 4, Ireland
E-mail: gallags@gmail.com

Present address:
S. Gallagher
Met Éireann,
Glasnevin, Dublin 9, Ireland

F. Dias
Centre de Mathématiques et de Leurs Applications,
École Normale Supérieure de Cachan, 94235, France

1 Introduction

The wave climate of the Northeast Atlantic possesses some of the highest wave energy levels in the world. Of late, a renewed interest in extracting this energy potential has occurred. Studies aimed at quantifying the variability of the wave climate and energy resource in areas of this region, over timescales of a decade or more, have been performed in recent years (for example Boudière et al, 2013; Charles et al, 2012; Dodet et al, 2010; Gallagher et al, 2013). In the operational wave forecasting community, increased attention is being paid to the nearshore (van der Westhuysen, 2012), awakened in part by the potential energy resource but also by an increased awareness of coastal hazards and their possible impacts on coastal communities. Improvements in ocean wave forecasting skill (Janssen, 2008) and the availability of high-quality global reanalysis datasets, now enable long term regional and local area wave hindcasts to be performed, downscaling to a high resolution in the nearshore.

Additionally, recent studies have shown that in nearshore locations, wave energy extraction levels could be commensurate to those found in the offshore (Folley and Whitthaker, 2009). In addition, the cost of transferring power onshore

and the accessibility for maintenance can be improved by the proximity to the coastline.

Most wave climate studies for Ireland, have targeted limited nearshore sites (Gallagher et al, 2013; Tiron et al, 2013) and also offshore locations on the Irish west coast (Cahill and Lewis, 2011; Curé, 2011; ESB, 2005; Rute Bento et al, 2012). The geomorphology of the Irish west coast is in fact quite heterogeneous and complex. This is likely to introduce significant variability in the wave energy resource for this region (Tiron et al, 2013). In order to investigate this variability, a high-resolution nearshore 34-year wave hindcast was carried out for Ireland, with a particular focus on the wave energy resource. To complete the wave climate picture, the entire coastline has been modelled, both the Atlantic coast and the eastern seaboard, where the majority of the population is located and where wind-seas dominate.

The wave climate is estimated using the third generation spectral wave model WAVEWATCH III version 4.11 (Tolman, 2009), the unstructured grid formulation (Roland, 2008). The wave model was forced with directional wave spectral data and 10m winds from the European Centre for Medium Range Weather Forecasts (ECMWF) ERA-Interim reanalysis, which is available from 1979 to the present (Dee et al, 2011; Persson, 2011).

The wave hindcast was validated with altimeter data from the CERSAT data base (Queffeulou and Croizé-Fillon, 2013) and with data from wave buoys located all around the coast of Ireland, in particular with buoys located in nearshore regions. Two such areas, which possess steep bathymetry gradients, and complex exposed rocky shorelines, are the southern part of Achill Island on the Co. Mayo coastline and an area centered at Killard point on the Co. Clare coast respectively. For these areas, wave buoy and Acoustic Doppler Current Profiler (ADCP) data for intermediate to shallow depths (50m or less) was obtained from the ESB's WestWave project (WestWave, 2013). Additionally, nearshore wave buoy data from other areas with more gentle bathymetric gradients (such as Broadhaven Bay, Co. Mayo) is used to validate the wave model.

2 Construction of the wave hindcast model

2.1 The digital elevation model

The quality of the bathymetric data used to build the computational grid greatly influences the accuracy of wave models in the nearshore. Historical seabed surveys have substantial uncertainties which only recently came under the scrutiny of the hydrographic community (Calder, 2006). These uncertainties are related to the survey methodology, interpolation of the scattered survey data and any changes in the seabed topography that may have occurred over time, after the bathymetric survey was carried out.

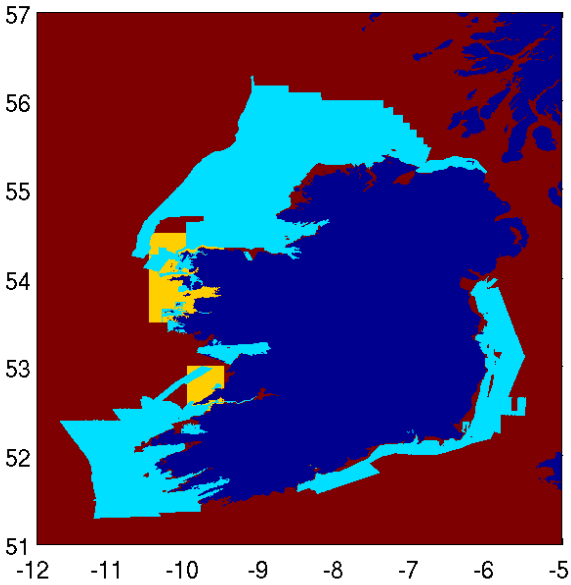

Fig. 1: Bathymetric datasets used in building the DEM for Irish coastal waters: INFOMAR (light-blue), UKHO (yellow), EMODnet (red) bathymetry and land (blue).

Modern and highly-accurate survey techniques such as light detection and ranging (LIDAR) or multi-beam echosounder (MBES) are currently used to map nearshore areas in campaigns such as the Integrated Mapping For the Sustainable Development of Ireland's Marine Resource (INFOMAR, 2006), which is a successor to the Irish National Seabed Survey (INSS), as described in Dorschel et al (2011). However, it may take several years for mapping of the Irish seabed to be completed.

In the interim, digital elevation models (DEMs) have to combine sets of data with varying degrees of accuracy and resolution. The level of accuracy of a DEM has an impact on the hydrodynamical model, and if not accounted for, could lead to erroneous interpretations of the results (Calder, 2006). Recent efforts have been made to construct DEMs with uncertainty estimates (Poti et al, 2012).

The final DEM for Ireland (see Figure 2) was obtained by merging three bathymetric sources (shown in Figure 1):

1. Vector data obtained from OceanWise Ltd., derived from the United Kingdom Hydrological Office (UKHO) admiralty charts. The quality of this data is not uniform, some of the surveys predate modern techniques;
2. The European Marine Observation and Data Network bathymetric dataset EMODnet (EMODnet, 2013). This dataset has a resolution of approximately 500m and blends bathymetric datasets from many sources in Europe. It is constantly updated with new surveys so the quality will continue to improve;

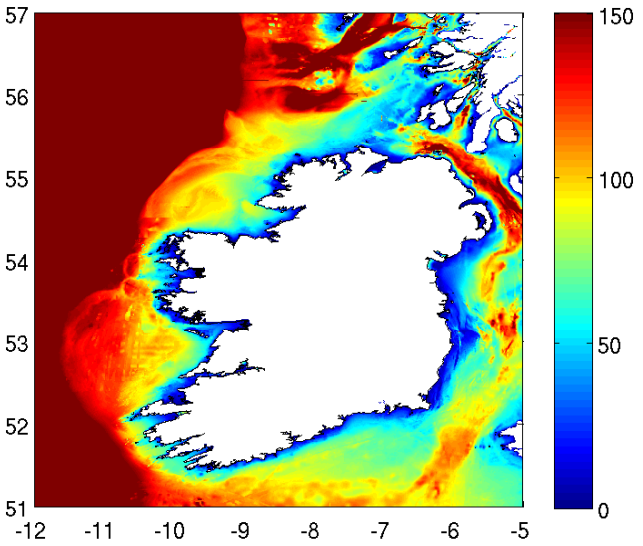

Fig. 2: DEM for Ireland (coastal waters) resulted from merging the bathymetric datasets depicted in Figure 1. Depth shown positive down.

3. High resolution MBES and LIDAR INFOMAR survey data. Approximately 50 gridded datasets, with resolutions from 2m to 80m were used.

The mismatch between the coarser datasets (EMODnet and UKHO) and high-resolution/high-quality INFOMAR dataset was evaluated on areas of overlap. Differences of more than 20m were observed in some nearshore locations (Tiron et al, 2013). The EMODnet dataset was found to be less accurate than the UKHO data in some nearshore areas on the west coast. Based on this observation, we have ranked the datasets in the order of accuracy (INFOMAR, UKHO and EMODnet).

To avoid artificial ridges at the boundaries between these datasets (which are likely to induce spurious refraction effects and numerical instabilities in the hydrodynamical model) a blending and smoothing procedure was then applied. The datasets were first gridded on a common grid with a resolution of 50m. Smoothing was applied if the original data was at a finer resolution than the target grid. The overlap areas were excluded from the coarse resolution datasets, based on the ranking mentioned above. Weights of 10, 5 and 1 were assigned to each of the datasets respectively, and a smoothing kernel with a variable radius based on depth was applied. The radius of smoothing varies between 100m (r_{min}) for depths smaller than 22m (h_0) to 2.5km (r_{max}) in the offshore area:

$$r_{min} + \frac{r_{max} - r_{min}}{2} \left[1 + \tanh\left(\lambda\left(h - h_0\right)\right)\right], \quad (1)$$

where $\lambda = 0.2$.

2.2 Wave model description

The wave model grid is an unstructured triangular grid with resolution varying from 250m in the nearshore to 10km in the offshore. The coast and island boundaries were derived from the Global Self-consistent Hierarchical High-resolution Shoreline (GSHHS) database (Wessel and Smith, 1996), the finest resolution version, smoothed and sampled at approximately 250m. Geo-referenced satellite imagery (LANDSAT, 2013) was used to correct the coastline and islands. It is worth noting that there are some areas on the west coast of Ireland where a significant mismatch between GSHHS and the shoreline can be seen (see for example Tiron et al, 2013).

The resulting grid has approximately 15,000 nodes with a maximum resolution of 250m in the nearshore (resolved to a depth of 5m from the shoreline). The outer boundary of the grid was chosen to align with ERA-Interim wave model grid points (see Figure 3). The boundary feeding was set at grid nodes on segments of the open boundary (in between, and at, the ERA-Interim grid points) where depths were larger than 90m. The spectral domain was discretized in 24 directions and 30 frequencies logarithmically spaced with an increment of 1.1 from 0.0345Hz, which coincides with the resolution of the ERA-Interim wave spectra used to force the model. The temporal resolution of the boundary feeding, and of the 10m ERA-Interim wind forcing fields, is 6 hours (the four standard synoptic times). The spatial resolution of the ERA-Interim winds is approximately 79km (Dee et al, 2011). The default WAVEWATCH III physical parameterisation switches were employed, with the exception of the *ST4* input and dissipation source term package (see Tolman (2009) for all switch details). This allows for improved parametrisation of source terms and dissipation as formulated in Ardhuin et al (2010). The model parameterisation formulation TEST451, as described in Ardhuin et al (2010), was selected. This parameterisation produced the smallest verification errors when tested in the study area. TEST451 also generally provides improved results at the global scale using ECMWF winds (Rascle and Ardhuin, 2013; Tolman, 2009).

Hourly field outputs were produced for standard mean wave parameters (significant wave height, standard wave periods, directions), the wave energy flux, spectral partitions parameters and wave-ocean layer parameters. Additionally, the directional spectra was saved every 3 hours at the buoy locations and at points on the 60m depth contour, as can be seen in Figure 3.

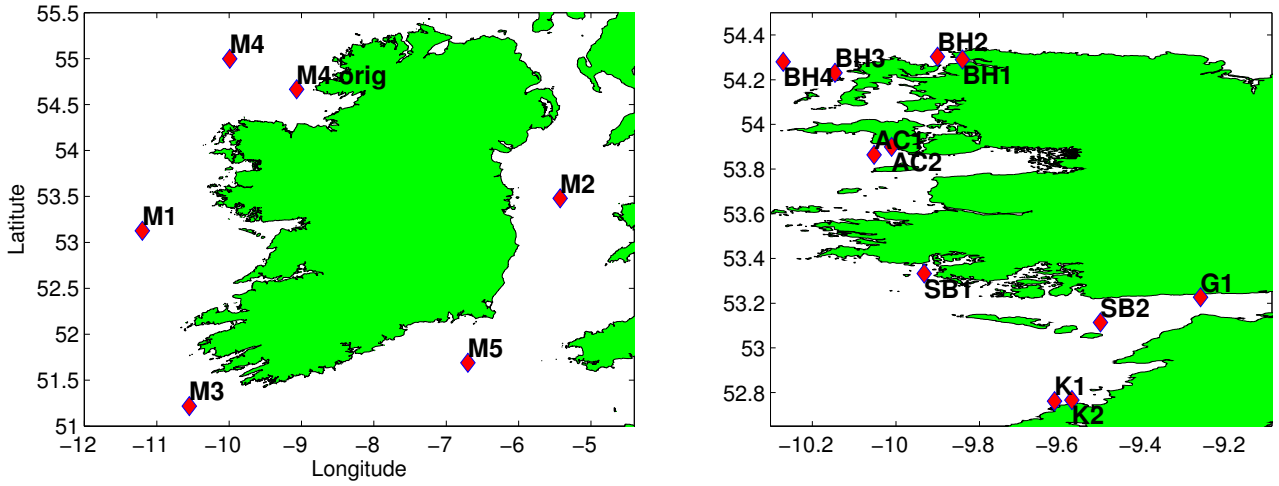

Fig. 4: Locations of the M-buoys from the Irish Marine Weather Buoy Network (left panel) and the nearshore buoys (right panel) used for validation of the wave model hindcast. The buoy availability ranges from time-periods of a few weeks to almost 10 years, as can be seen in Table 1.

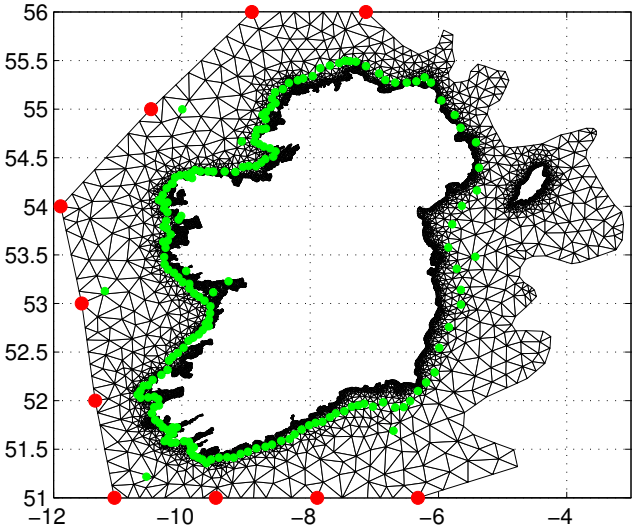

Fig. 3: The wave model grid. Red: ERA-Interim wave model points used for boundary feeding. Green: points where 3-hourly directional spectra outputs were generated.

Table 1: Buoy location depth and duration of the time-series used in comparison with model data. Buoys listed in order of depth.

Buoy	*Location*	*Depth* (*m*)	*Period* (*mm*/*yyyy*)
M3	SW of Mizen Head	155	01/2003 - 12/2012
M1	W of Aran Isl.	140	03/2001 - 12/2007
BH4	W of Belmullet	100	05/2012 - 12/2012
M2	E of Lambay Isl.	95	05/2003 - 12/2012
M4	Donegal Bay	72	04/2003 - 11/2012
M5	SE Coast	70	10/2004 - 12/2012
BH3	W of Belmullet	56	12/2009 - 01/2012
K1	Killard Point	51	11/2011 - 01/2012
AC1	Achill Isl.	43	11/2011 - 08/2012
BH1	Broadhaven Bay	38	01/2009 - 10/2009
K2	Killard Point	36	08/2012 - 12/2012
SB2	E of Aran Isl.	28	01/2010 - 06/2010
G1	Galway Bay	22	05/2008 - 01/2012
AC2	Achill Isl.	21	11/2011 - 01/2012
SB1	Mace Head	18	04/2909 - 09/2009
BH2	Broadhaven Bay	11	06/2006 - 07/2009

3 Validation of the wave model

3.1 Wave buoys

The wave model was validated with data from 17 different wave buoys located around the Irish coastline as shown in Figure 4. These buoys vary in depth from 155m to 11m, as described in Table 1. It should be noted that the Irish Marine Weather Buoy Network, maintained by Met Éireann and the Marine Institute (M.I., 2013), has only been in operation since 2001, when the first buoy was deployed. Additionally, buoy data in the nearshore has only become available in recent years, predominantly on the west coast, targeting potential wave energy testing and deployment sites, as it can also be seen Table 1.

The comparison between model and observations using statistical quality indexes for significant wave height (Hs), period and direction is summarised in Table 2. Taylor diagrams (Taylor, 2001) for Hs, period and direction are shown in Figure 5. A separation of the results by depth is shown for clarity, with offshore buoys (depths $>$ 60m) shown with black symbols and nearshore buoys (depths $<$ 60m) shown with red symbols. Generally, the model appears to perform well when compared to the measured values. The correlation

Table 2: Comparison between the model and buoy for significant wave height (Hs), period and direction: the mean of the buoy (X), the bias, the root-mean square error (RMSE), the correlation coefficient (R) and the scatter index (SI) are shown. Where possible the zero-crossing period and mean direction were used. In some locations only the peak period or peak direction was available. All directional error statistics were calculated using the circular statistics toolbox from Berens (2009). *(* denotes where comparisons were between the buoy and model peak period or peak direction, respectively.)*

	Hs :					**Period** :					**Dir** :				
Buoy	*X* (*m*)	*Bias* (*cm*)	*RMSE* (*cm*)	*R*	*SI* (%)	*X* (*s*)	*Bias* (*s*)	*RMSE* (*s*)	*R*	*SI* (%)	*X* (*deg*)	*Bias* (*deg*)	*RMSE* (*deg*)	*R*	*SI* (%)
M3	2.86	-4	45	0.95	16	6.9	0.3	0.8	0.87	11	275	5	13	0.95	15
M1	2.94	-15	46	0.96	16	7.3	0.3	0.9	0.86	12	-	-	-	-	-
BH4	2.87	5	38	0.96	13	6.7	0.2	0.6	0.92	8	292*	9	20	0.7	29
M2	1.19	15	31	0.94	25	4.5	0.9	1.2	0.65	26	189	-15	24	0.77	14
M4	3.11	-1	39	0.97	13	7	0.2	0.7	0.98	19	275	2	13	0.94	15
M4(old)	2.34	-24	55	0.94	23	6.7	0.3	0.9	0.84	13	-	-	-	-	-
M5	1.81	-3	38	0.94	21	5.5	0.1	0.8	0.82	15	231	-6	18	0.84	14
BH3	2.77	11	40	0.97	15	7	0.2	0.7	0.89	10	296*	7	16	0.69	25
K1	4.57	31	53	0.97	12	8	0.0	0.7	0.88	7	291*	4	9	0.74	13
AC1	2.32	-14	34	0.98	15	6.3	-0.1	0.7	0.91	11	270*	5	13	0.68	14
BH1	1.90	2	31	0.97	16	6.2	0.1	0.9	0.86	14	317	4	11	0.83	25
K2	2.44	20	40	0.96	16	6.7	0.0	0.7	0.90	11	292*	-0.5	9	0.75	13
SB2	0.62	-5	17	0.89	27	4.3	-0.4	1.9	0.61	43	259	12	29	0.65	29
G1	0.75	7	18	0.94	25	4.1	-0.3	1.5	0.60	6	-	-	-	-	-
AC2	3.79	-6	43	0.95	11	12.3*	-0.5	1.5	0.76	12	260*	6	12	0.45	12
SB1	0.85	-36	44	0.95	52	4.7	-0.4	1.1	0.71	23	230	6	12	0.70	9
BH2	0.36	1	8	0.97	15	-	-	-	-	-	-	-	-	-	-

coefficients for significant wave height are all over 0.94 with the exception of 0.89 for the SB1 buoy (located in Galway Bay, in the shadow of the Aran Islands). A significant bias in Hs can be seen for SB2 (over 40%). This buoy is located in an area where only EMODnet bathymetry was available, with shallow depths of under 20m. Interestingly the correlation coefficient is very good for this location, however the observed discrepancy raises questions regarding the accuracy of the bathymetry dataset in this region and in particular for these depth ranges.

3.2 Altimeter data

Satellite-derived wave data can provide an additional method to verify the wave models performance. Altimeter wave data is reliable only in the open ocean, up to tens of km from the coast (data in the coastal zone is often discarded). Recent work has been carried out to improve satellite derived measurements in the nearshore coastal zone, such as the COASTALT Project (COASTALT, 2014). Currently however, only altimeter data from the open ocean can provide reliable wave measurements. Altimeter data can provide a way to further validate the hindcast in areas with little or no buoy records available, as is the case on the eastern seaboard of Ireland, where presently there is only one buoy (M2). This data provides a good spatial description of the wave climate, although the temporal resolution is low due to the long repeat cycle orbits of the various satellites (as detailed in Table 3). The CERSAT altimeter database was used to compare with model results (CERSAT, 2013). The CERSAT database data was obtained from the Centre de Recherche et d'Exploitation Satellitaire (CERSAT), at Ifremer, Plouzané, France. They were produced in the framework of the Globwave project (GlobWave, 2013), funded by the European Space Agency (ESA). These altimeter-derived measurements have been calibrated and corrected in previous work by Queffeulou and Croizé-Fillon (2013). This data provides an almost continuous 21 year record with which the wave model was compared. The different altimeter missions include ERS-1&2, TOPEX-Poseidon, GEOSAT Follow-ON (GFO), Jason-1, Jason-2, ENVISAT and Cryosat-2. The tracks over the wave model area for all of 2006 can be seen in Figure 6.

Altimeters typically yield one second mean values, with a 6-7km resolution (GlobWave, 2013). The wave model hindcast has a varying resolution of approximately 10km (offshore) to 250m (in the very nearshore) and a temporal resolution of one hour. In order to compare Hs from the two datasets, the nearest model Hs was interpolated to the position of the altimeter tracks in space and time. The results of this spatio-temporal comparison between the satellite data and the model data (interpolated to collocate along the satellite tracks), are summarised in the statistical quality indexes shown in Table 4. These global statistics show a low model bias of 7cm in Hs. This corresponds to a relative bias (normalised by the observed mean) of only 3% and very good agreement overall between the model and satellite data. Fur-

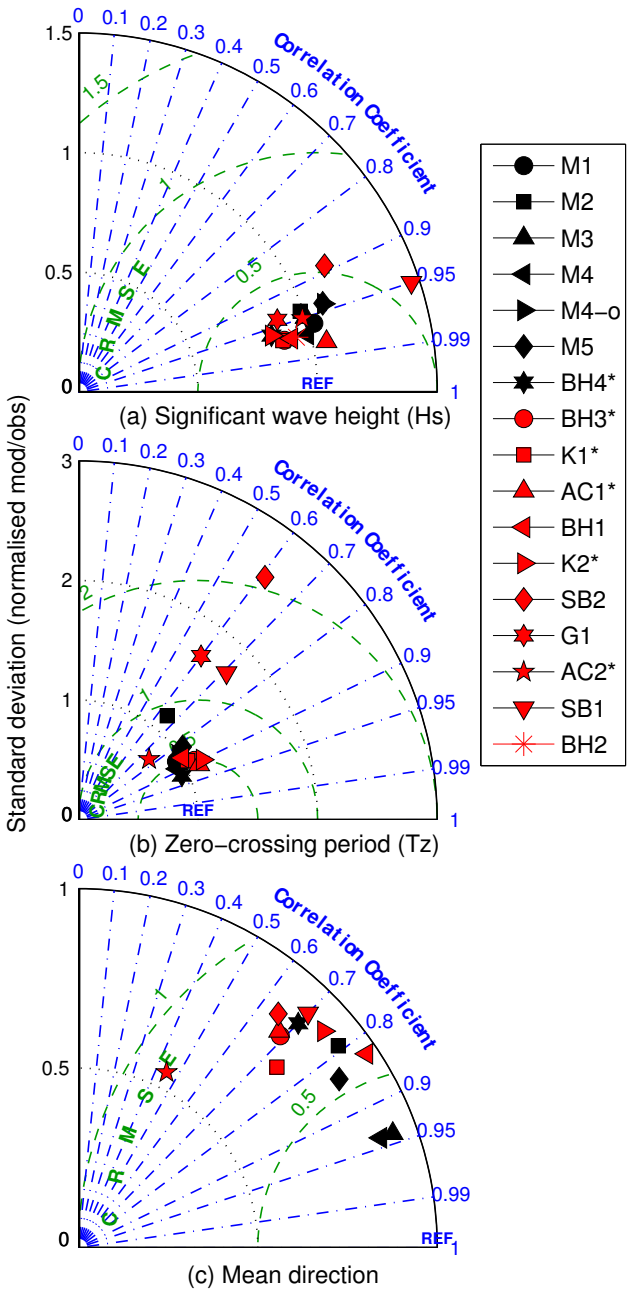

Fig. 5: Top panel (a) - Hs; middle panel (b) - zero-crossing period; and bottom panel (c) - mean direction Taylor diagrams (showing a statistical comparison in terms of correlation, centered root mean square error (CRMSE) and the ratio of standard deviation) between the buoy observations and the model. Further statistical comparisons can be seen in Table 2. Additional separation of the results by depth can be seen with offshore buoys with depths $>$ 60m shown with black symbols and nearshore buoys with depths $<$ 60m shown in red. *(* denotes where comparisons were between the buoy and peak direction instead of mean direction, with the exception of AC2 buoy, where the comparison was between the model and both peak period and peak direction from the buoy, respectively.)*

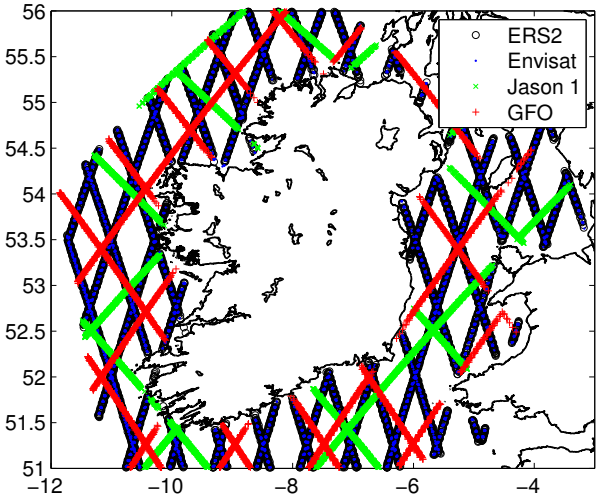

Fig. 6: Satellite altimeter tracks over the wave model area during 2006.

Table 3: Summary of the altimeter data extracted from the CERSAT database that was used to validate the wave model hindcast. Details of the calibrations applied to the dataset can be found in Queffeulou and Croizé-Fillon (2013).

Satellite	*Repeat Cycle* (*Days*)	*Period* (*mm/yyyy*)
ESA ERS-1	35	08/1991 - 06/1996
ESA ERS-2	35	05/1995 - 07/2011
ESA Envisat	35 (pre 10/2010) 30 (post 11/2010)	05/2002 - 04/2012
CNES / NASA TOPEX / Posidon	10	09/1992 - 10/2005
CNES / NASA Jason-1	10	01/2002 - present
CNES / NASA Jason-2	10	07/2008 - present
US Navy / NOAA GFO	17	01/2000 - 09/2008
ESA / NOAA CryoSAT-2	30 (pseudo cycle)	01/2012 - present

ther analysis and a breakdown by satellite can be seen in Figure 7 which shows a Taylor diagram of the model versus observed (satellite altimeter) data along with a quantile-quantile (Q-Q) plot and a histogram of distribution of the difference/error (altimeter minus wave model at each of the track points) of the global comparison between altimeter and model, from the period 1991-2012. As can be seen from the Q-Q plot in Figure 7b, the model begins to slightly underestimate Hs values above 8m. The histogram of differences between observed (altimeter) and model (Figure 7c) also shows the wave model slightly underestimating the value for Hs, as can be seen by the heavier positive tail of the histogram (histogram in 0.2m bins).

A regional examination of the model performance was undertaken, to take into account the very different wave climate regimes that exist around Ireland between the Atlantic ocean (swell dominated, mean Hs of 2.69m) and the Irish

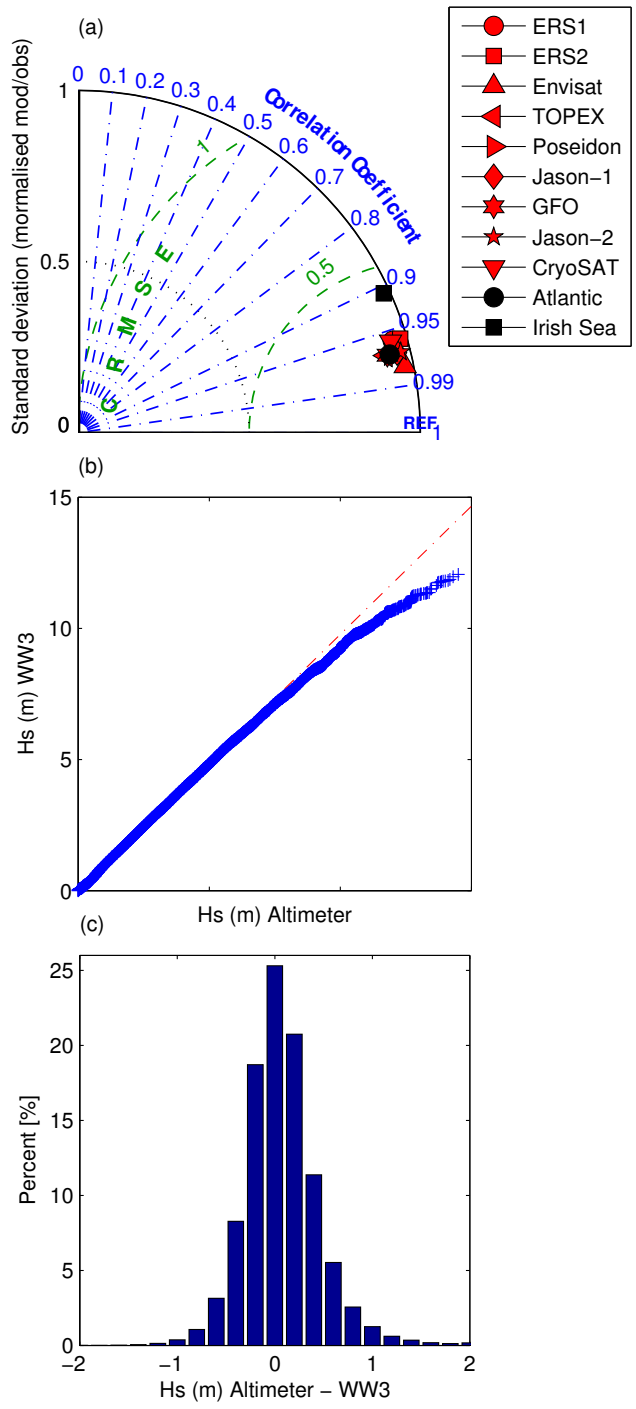

Fig. 7: Top panel (a): Taylor plot of the wave model versus the CERSAT satellite altimeter database (global comparison). Middle panel (b): Q-Q plot of the global satellite altimeter data versus Hs of the wave model (WW3). Bottom panel (c): a histogram of the difference between altimeter and model for Hs at the collocated track points.

Table 4: Global comparison from 1991-2012 (21 years) between the model and satellite altimeter data from the CERSAT database for significant wave height (Hs): the mean of the satellite (X), the bias, the root-mean square error (RMSE), the correlation coefficient (R) and the scatter index (SI) are shown. See Table 3 for details of the different altimeter campaigns.

Hs	*Number of Points*	*X* (*m*)	*Bias* (*cm*)	*RMSE* (*cm*)	*R*	*SI* (%)
All areas	523471	2.29	7	39	0.97	17
Atlantic & Celtic Sea	376099	2.69	5	39	0.97	15
Irish Sea	144453	1.29	12	38	0.91	29

Sea (wind-sea dominated, mean Hs of 1.29m). The different wave climate regimes are discussed further in Section 4 and can be seen in Figure 10. The Irish Sea area was defined as the part of the wave model east of $-6.4°$W in longitude, and north of $51.75°$N and south of $55.25°$N in latitude. The Atlantic and Celtic Sea region was defined for the purposes of the comparison as all areas except for the area that is both east of $-6.4°$W and north of $51.75°$N (i.e the Irish Sea and Firth of Clyde).

Looking at Table 4, the relative bias for the Atlantic and Celtic Seas regions covered by the wave model is less that 2%. The statistical comparison for the Irish Sea (Table 4) shows a much larger relative bias of over 9% (12cm). This is consistent with the results of the M2 buoy comparison with the model, where the bias of 15cm, or a relative bias of over 12% as can be seen in Table 2. A lower correlation and a much larger scatter index and spread in the data can also be found in the Irish Sea area as can be seen in Figure 8 where scatter plots of the Irish Sea and Atlantic model results versus the altimeter data is shown for Hs. The fact that the wind forcing for the hindcast has a relatively coarse resolution of 79km, and might therefore be too coarse to capture some localised mesoscale wind effects, especially due to orography, could explain the small drop in model performance in the Irish Sea region. These forcing wind fields would need to be of sufficient resolution to reflect the small scale features associated with the coastline of the Irish Sea basin and the sheltering effects of bays and islands. A downscaling of the wind forcing, to capture better this wind-sea dominated area has been shown to improve the model performance. For details please see the report by Dias et al (2013).

To examine further some of the statistical quality indexes spatially, altimeter and wave model Hs results already collocated (spatially and temporally) along the satellite tracks were then interpolated to a regular grid by averaging along the tracks in a $0.2°$ latitude by $0.2°$ longitude grid. Using this collocated data the overall mean Hs (over the 21 year period of altimeter wave data), the relative bias and normalised root

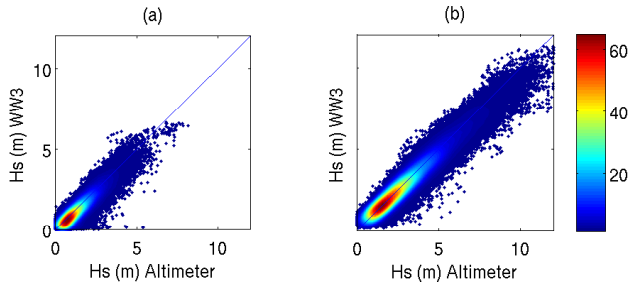

Fig. 8: Scatter diagrams of altimeter versus model Hs (m). Model data interpolated onto satellite tracks. Colours indicate density of points. (a): Irish Sea area. (b)l: Atlantic and Celtic Sea area.

mean square error (nRMSE) can be seen in a spatial context in Figure 9 using quality index maps. (Similar methods have been employed as part of the GlobWave project by Appendini and Camacho (2012), collocating data to examine spatial quality index maps and by Liberti et al (2013), although no temporal or spatial interpolation was carried out as the nearest grid cell was used for statistical comparison.)

Comparing the overall altimeter mean Hs in Figure 9a to the annual mean shown in Figure 11 from the analysis of the wave model hindcast Hs, the overall pattern is similar. The relative bias and nRMSE shows the lower performance of the hindcast in the Irish Sea. As discussed previously, this could be due to the relatively low resolution forcing wind fields, which are unable to capture wind-sea growth in the wind dominated Irish Sea. Looking at the western seaboard, the relative bias is generally less than $\pm 3\%$. This is consistent with Table 2 where the biases for buoys on the west coast vary between negative and positive, although the variability and magnitude of the relative bias is larger when comparing the buoy and model data. For example, the BH3 buoy has a positive relative bias of 4% while the M1 buoy has a negative relative bias of -5%. The largest relative biases looking at Figure 9 are on the south coast in the Celtic Sea region which shows a negative relative bias (mostly between -1 to -4%) overall. The M3 buoy located in this region (see Figure 4 for location and Table 2 for quality index statistics), was found to have a negative relative bias of -1.4%, consistent with the findings of the re-gridded collocated model and altimeter data in Figure 9.

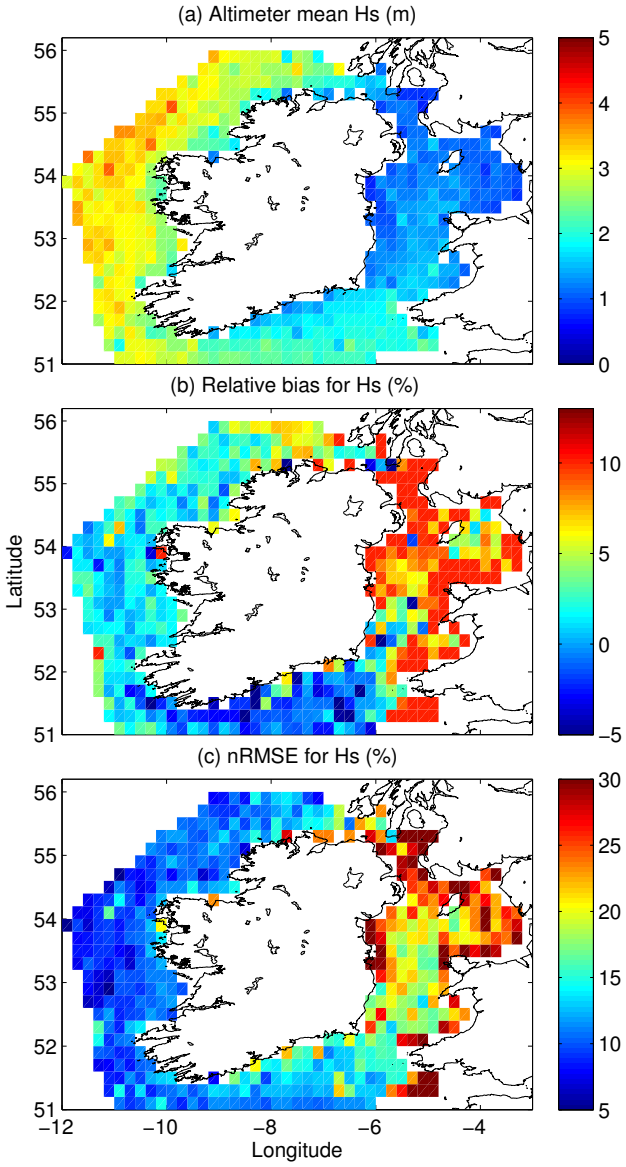

Fig. 9: Spatial quality index maps for Hs (m) of the collocated CERSAT satellite altimeter data (observed) and the wave model hindcast (WW3) 1991-2012. Top panel (a): Mean Hs (m). Middle panel (b): Relative bias (%). Bottom panel (c): Normalised root mean square error (%).

4 Characterisation of the present wave climate of Ireland

In this section the wave climate of Ireland during the period 1979-2012 is characterised, based on the hindcast introduced in the preceding sections of this article. The goal is to compose an overall picture of wave climate variability around the Irish coast and in particular to contrast the Atlantic west and southern coasts to the milder wind-dominated Irish Sea coast. As such, the details gained in describing the wave climate in the nearshore are perhaps not immediately apparent in this analysis. As shown in Section 3.1, the hindcast results compare favourably with measurements from buoys in water depths as low as 20m, and thus offer a detailed picture of the nearshore wave climate of Ireland.

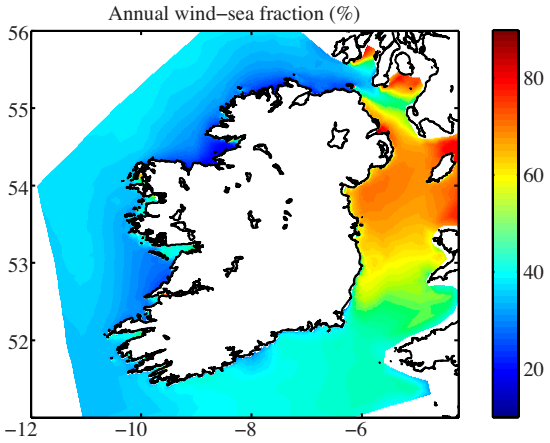

Fig. 10: Average of the wind-sea fraction of the wave-energy spectra for the period 1979-2012 (%).

Further analysis focusing on regions close to the coastline will be performed in the near future.

A look at the overall average of the wind-sea fraction of the wave energy spectra (presented in Figure 10) reveals three areas with distinct wave climate regimes. The local winds are responsible for more than 60% of the wave energy in the Irish Sea. On the southern coast, the swell and wind-sea components are equally represented, whereas the west coast is swell-dominated, with the exception of areas where the Atlantic swells are attenuated by islands or in bays and inlets. It is interesting to note that the hindcast quality appears to degrade with higher wind-sea fraction values (see for instance Figure 9, where spatial quality index maps for the model performance by comparison to satellite data are shown). This fact offers supplementary evidence for the insufficient spatial resolution of the forcing wind fields employed in the current hindcast as discussed previously in Section 3.2.

4.1 Seasonal means and interannual variability

In the following section, we focus on the spatial, seasonal and interannual variability of mean wave parameters of interest. The annual and seasonal means for significant wave height are shown in Figure 11, left panels. The right panels show the normalised standard deviation of the annual means (%) which quantifies the variability from year to year.

The overall means display a pronounced spatial variation around the coast: from 3m off the west coast to less than 1m in the Irish Sea. The southwest to the northwest exhibits the largest levels of Hs and, in fact, these patterns are preserved for all seasons. The largest values of Hs can be seen in winter off the west coast (close to 5m). In contrast, mean Hs values do not exceed 2m on the Irish Sea coast in any season. The spring and autumn means are very similar (and commensurate with the overall annual mean). This is in fact the case for all mean wave parameters.

The Irish wave climate presents significant interannual variability in terms of Hs: overall less than 15% for the annual means but over 25% in winter and spring. On the Atlantic coast the interannual variability is more pronounced in the nearshore.

Figure 12 displays the annual and seasonal means for the wave power per metre of wave crest CgE (upper panels) and the normalised standard deviation of the yearly CgE means, % (lower panels). The focus is on the west coast, since the power levels typically seen on the south and east coasts are quite reduced and thus these areas are not targeted as potential sites for Wave Energy Converter farms.

In winter, the Atlantic coast is exposed to highly energetic sea states (over 100kW/m), which do not dissipate significantly until very close to the shoreline. It is important to note in this context that wave energy converters (WECs) are typically designed to extract energy up to a certain level above which they are not safe to operate. A more accurate measure of the wave energy resource would have to take into account these limitations (Folley and Whitthaker, 2009). It is thus expected that the exploitable energy levels in winter are substantially smaller. The decrease in energy levels from winter to summer is quite dramatic, even though on the west coast energy levels of up to 20kW/m are maintained in summer months. For CgE, the variability from year to year is markedly larger than for Hs, as evident in Figure 12 - around 20% for the annual mean and over 50% in spring.

The Irish wave climate exhibits little seasonal variability in terms of direction. In Figure 13 the overall average of the mean and peak wave direction for the period 1979-2012 is displayed. (The circular mean was evaluated for all directional quantities.) The predominant incoming wave direction on the Atlantic coast is west to southwest (with only a slight 10-20° southerly shift from the west direction). In the northwest of Ireland and in a small area from the Dingle peninsula up to the Loop head, the predominant direction is from the west.

On the Irish Sea coast, waves come predominantly from a southerly direction. The same mean direction can be seen on the southern coast of Ireland. The average peak direction is very similar to the mean direction. However, a small northerly shift in peak direction with respect to the mean direction, can be seen off the northwest coast.

4.2 Correlation with atmospheric teleconnection patterns

As the generating mechanism of ocean surface waves consists in surface winds, global atmospheric circulation patterns and wave climate characteristics are intimately connected.

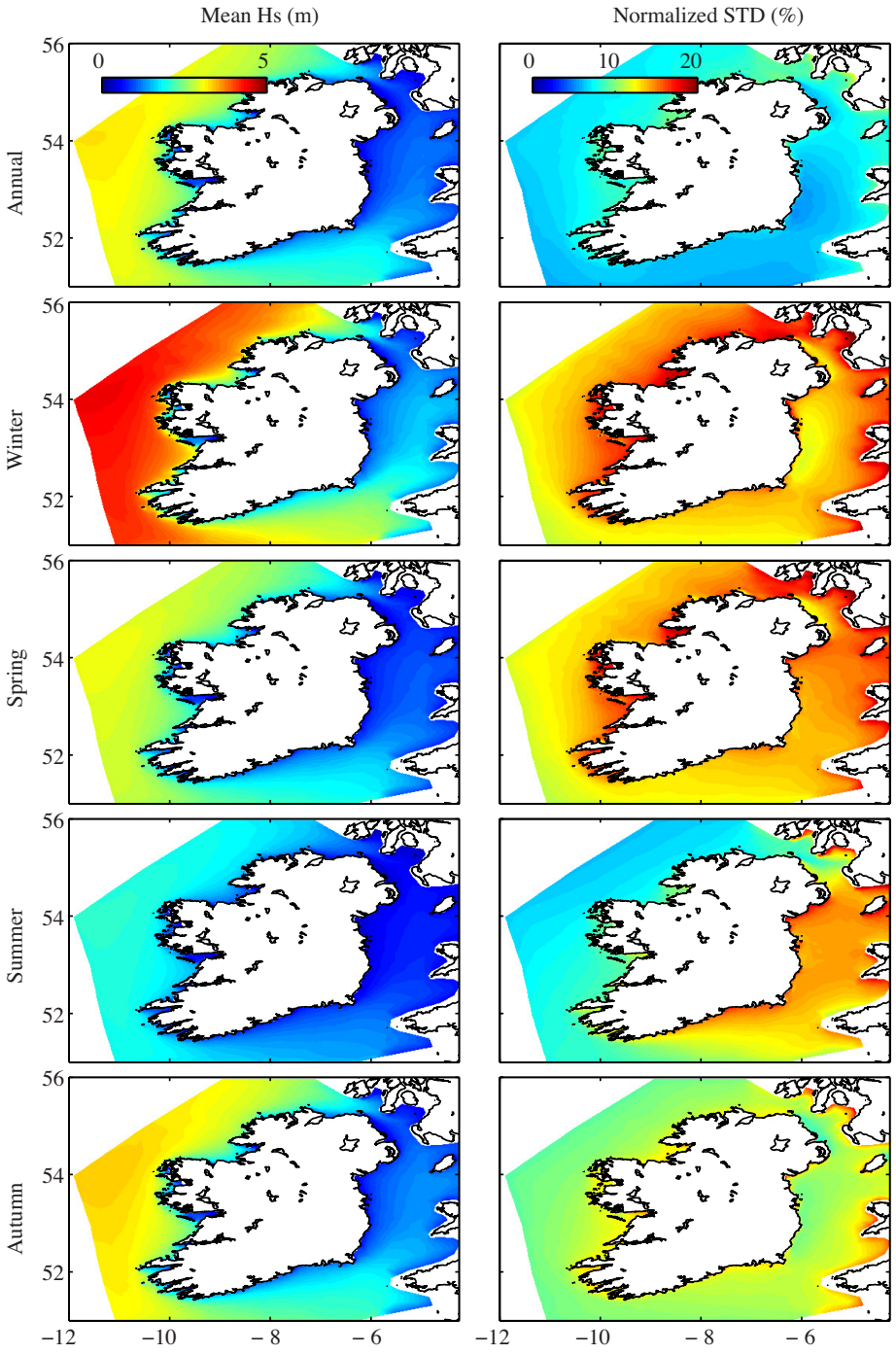

Fig. 11: Significant wave height (m) for the period 1979 to 2012. Left panels: annual and seasonal means. Right panels: normalised standard deviation of the yearly means (%) which is a measure of the interannual variability.

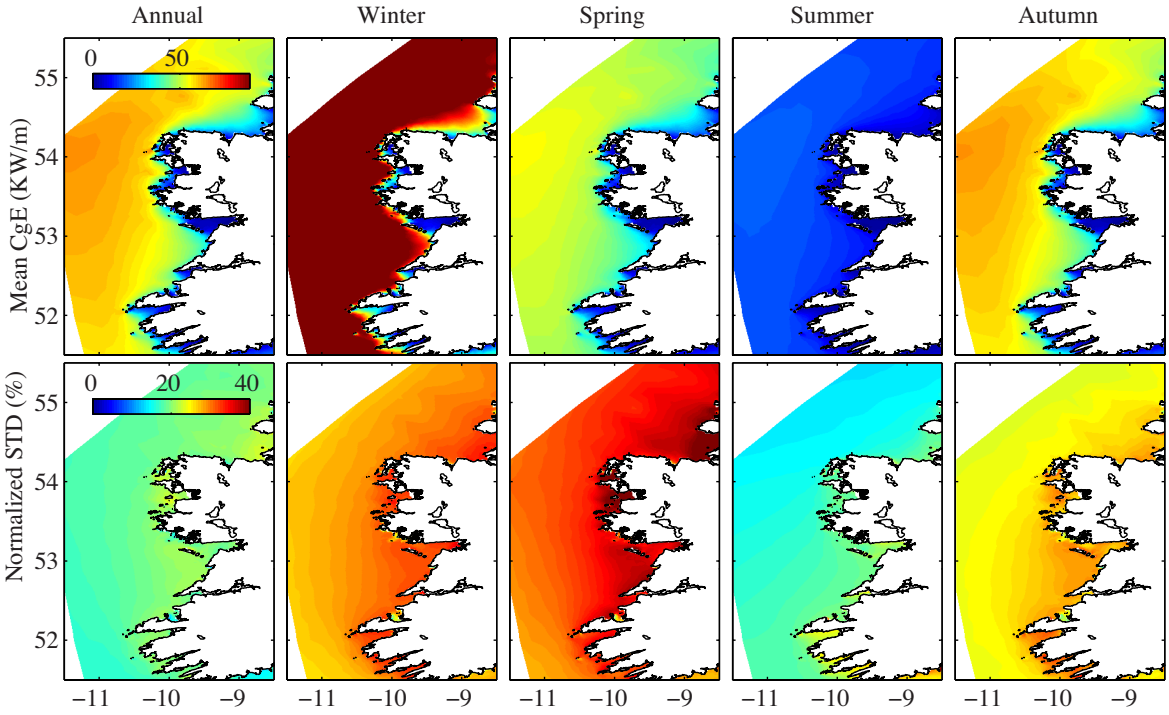

Fig. 12: Wave energy flux (kW/m of wave crest) for the period 1979 to 2012. Upper panels: annual and seasonal means. Lower panels: normalised standard deviation of the means (%) which is a measure of the interannual variability of the wave energy resource.

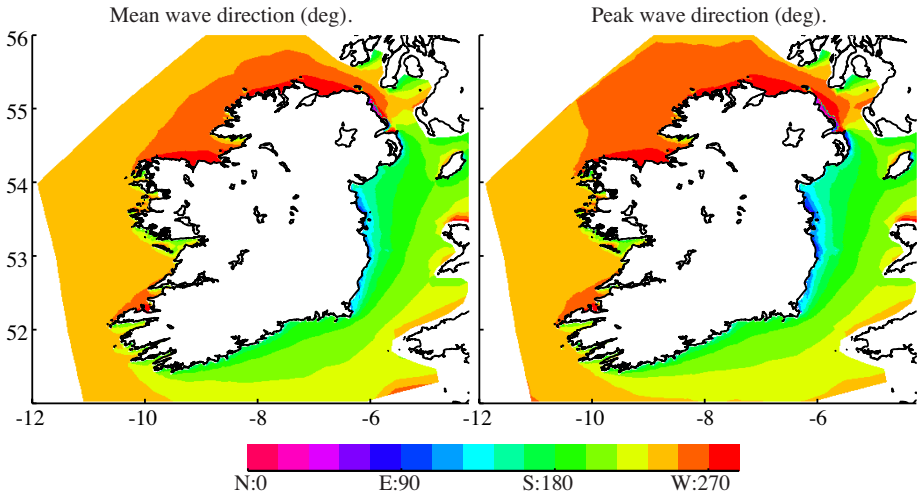

Fig. 13: Directionality of the Irish wave climate for the period 1979 to 2012. Left panel: annual average mean wave direction (deg). Right panel: annual average peak wave direction (deg). *Directions are given in the meteorological convention: 0° corresponds to waves coming from North, 90° corresponds to waves coming from East.*

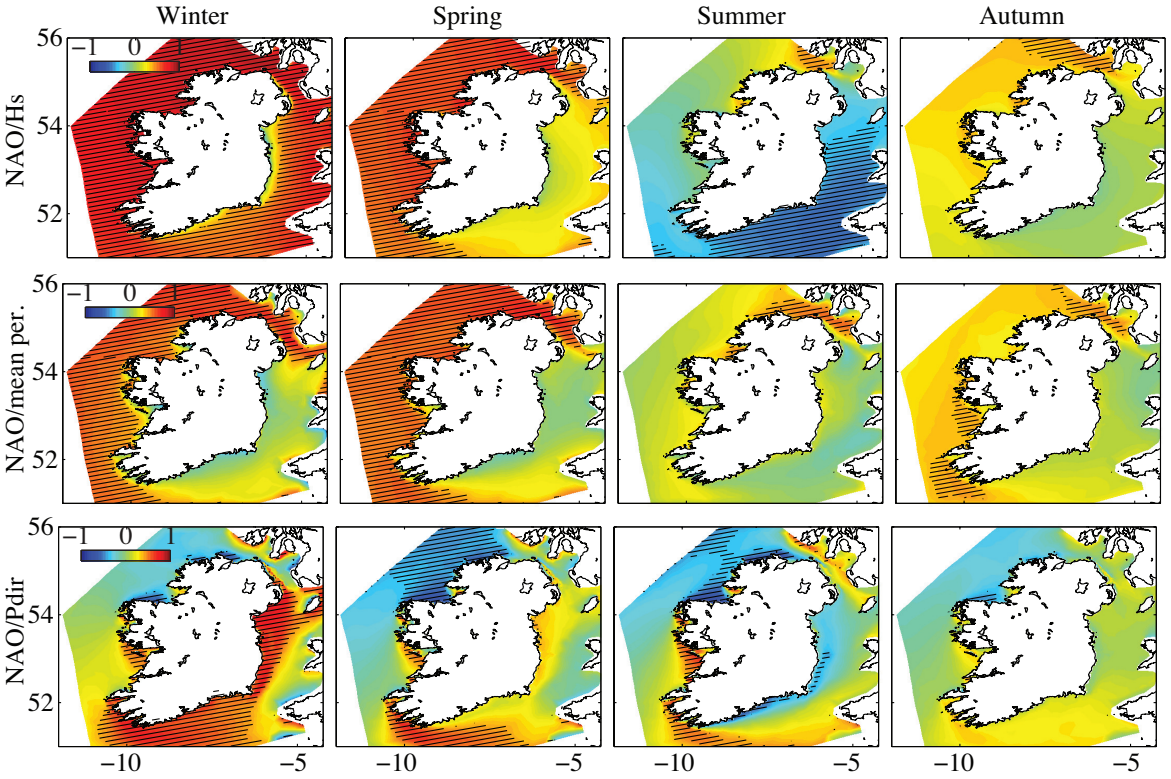

Fig. 14: Pearson correlation coefficient between NAO and seasonal averages of significant wave height, mean period and peak direction. Hatched: areas with correlation significant at higher than 95% by *t*-test.

The strong interannual variability of the Irish wave climate (evidenced in Figures 11 and 12) can be in fact linked to larger scale atmospheric circulation patterns. Several studies have identified strong correlations between the Atlantic wave climate averages and the various teleconnection indices, such as the North Atlantic Oscillation (NAO) or the East Atlantic teleconnection pattern (EA) (Barnston and Livezey, 1987) at the whole Atlantic basin scale (Wang and Swail, 2001, 2002) and also for the Northeast Atlantic region (see for example recent studies by Bertin et al, 2013; Charles et al, 2012; Dodet et al, 2010; Le Cozannet et al, 2010).

Local winds play an important role in the Irish wave climate, in particular in the Irish Sea (as Figure 10 shows). At the same time, the swells generated in the North Atlantic basin, which propagate long distances before reaching Ireland are prevalent on the west coast. As a consequence, the wave climate around the Irish coast is quite heterogeneous. With this in mind, we evaluate the correlation between the predominant patterns in the North Atlantic region (NAO and EA) and the Irish wave climate, contrasting the Atlantic and Irish Sea coasts.

In Figure 14 the correlation between seasonal averages and NAO (retrived from the Climate Prediction Center NOAA, 2013) for Hs, wave energy period (Tm) and wave peak direction (Pdir) are displayed. The areas with correlation significant at more than 95% by Student *t*-test are hatched for clarity. As discussed by Bacon and Carter (1993), correlation coefficients greater than 0.5 signify a relatively strong connection between the wave climate and teleconnection patterns.

As can be seen in this figure, the Irish wave climate is highly influenced by the NAO in winter. The significant wave height is directly correlated with NAO, with correlation coefficients exceeding 0.7 over most of the study area extent, with the exception of the nearshore eastern seaboard. These findings are consistent with similar studies (such as those mentioned previously), which found positive phases of the NAO index to be associated with increased wave heights in the Northeast Atlantic in winter.

A significant positive correlation can be seen for the energy period on the west and northern coasts in winter, indicating an increase in energy period associated with positive NAO phases in these regions. For the peak wave direction, a statistically significant positive correlation is present on the southern and east coasts and in the Galway bay on the west coast, corresponding to a northerly shift with increasing NAO indexes. The positive correlation of wave heights and energy period with the NAO index persists on the west and northern coasts in spring. The summer and autumn wave climate is not impacted significantly by the NAO phase, with

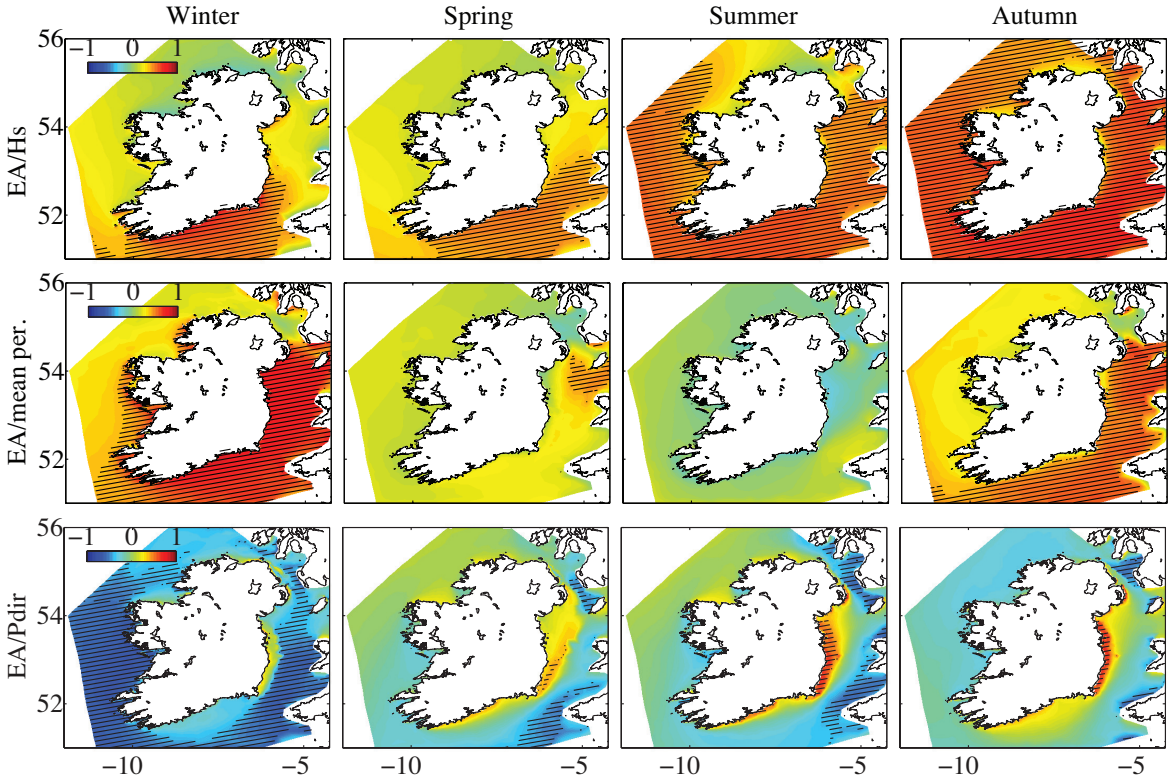

Fig. 15: Pearson correlation coefficient between EA and seasonal averages of significant wave height, mean period and peak direction. Hatched: areas with correlation significant at higher than 95% by *t*-test.

the exception of a negative correlation for significant wave heights in the southwest in summer.

Overall, the influence of the NAO on the Irish wave climate appears to be more significant than in other North-east Atlantic regions (for example as estimated by Charles et al, 2012, in the Bay of Biscay), in particular in winter and spring.

The correlation maps between the wave climate seasonal averages (Hs, Tm) and Pdir) and the EA teleconnection pattern (retrieved from Climate Prediction Center NOAA, 2013) are displayed in Figure 15, with areas of correlation, significant at more than 95% by Student *t*-test, shown with hatching for clarity. The most consistent connection with the EA index can be seen in autumn, in particular in the Irish Sea region and on the southern coast, where statistically significant positive correlations with the EA phase are present for both significant wave height and mean period. For this season, a positive correlation for the significant wave height can also be seen on the western coast. The winter season presents significant correlations with the EA index for Hs and Tm on the southern coast. At the same time, the peak direction is inversely correlated with the EA phase, implying a southerly shift for increasing EA indexes. For spring and summer, the mean period and peak direction are not significantly affected by the EA phase. Significant positive correlations with Hs can be seen in summer in the west, south and east, and in spring on the southern coast.

In conclusion, the EA appears to have less of an impact on the wave climate of Ireland in comparison with the NAO. The strongest correlation with the EA occurs in the autumn, and persists throughout the seasons in the south and the south-east. This is in contrast to the NAO which dominates the wave climate on the west coast, particularly in winter and spring.

We conclude this section by taking a closer look at the impact of the winter NAO phase (depicted in Figure 16) on the winter wave climate around the Irish coast. To this end, we evaluate the winter average significant wave height over the entire study area and the wave-variance density spectra at 5 points around the coast (depicted in panel (a) of Figure 17) to contrast:

- the years corresponding to the maximum and minimum NAO phase that occurred during the 1979-2012 period (1993 NAO+ and 2010 NAO− respectively) – results summarized in Figure 17;
- the average over the years with local NAO maxima and local NAO minima – results summarized in Figure 18.

The differences in wave heights between winter 1993 (NAO+) and 2010 (NAO−) (shown in panels (a) and (b)

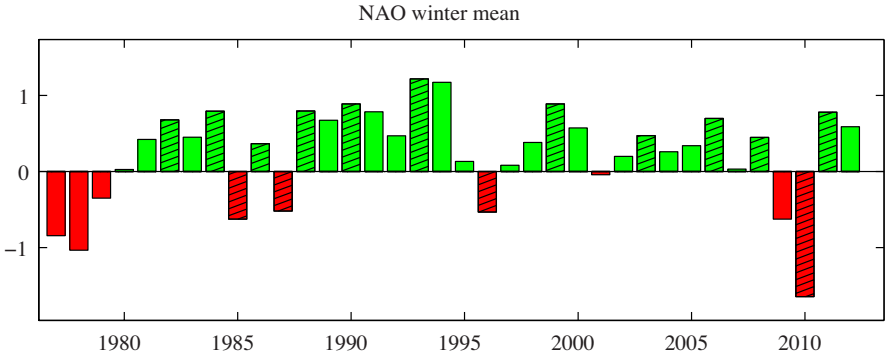

Fig. 16: Averaged winter (December, January, February) NAO index. Hatched: local minima/maxima.

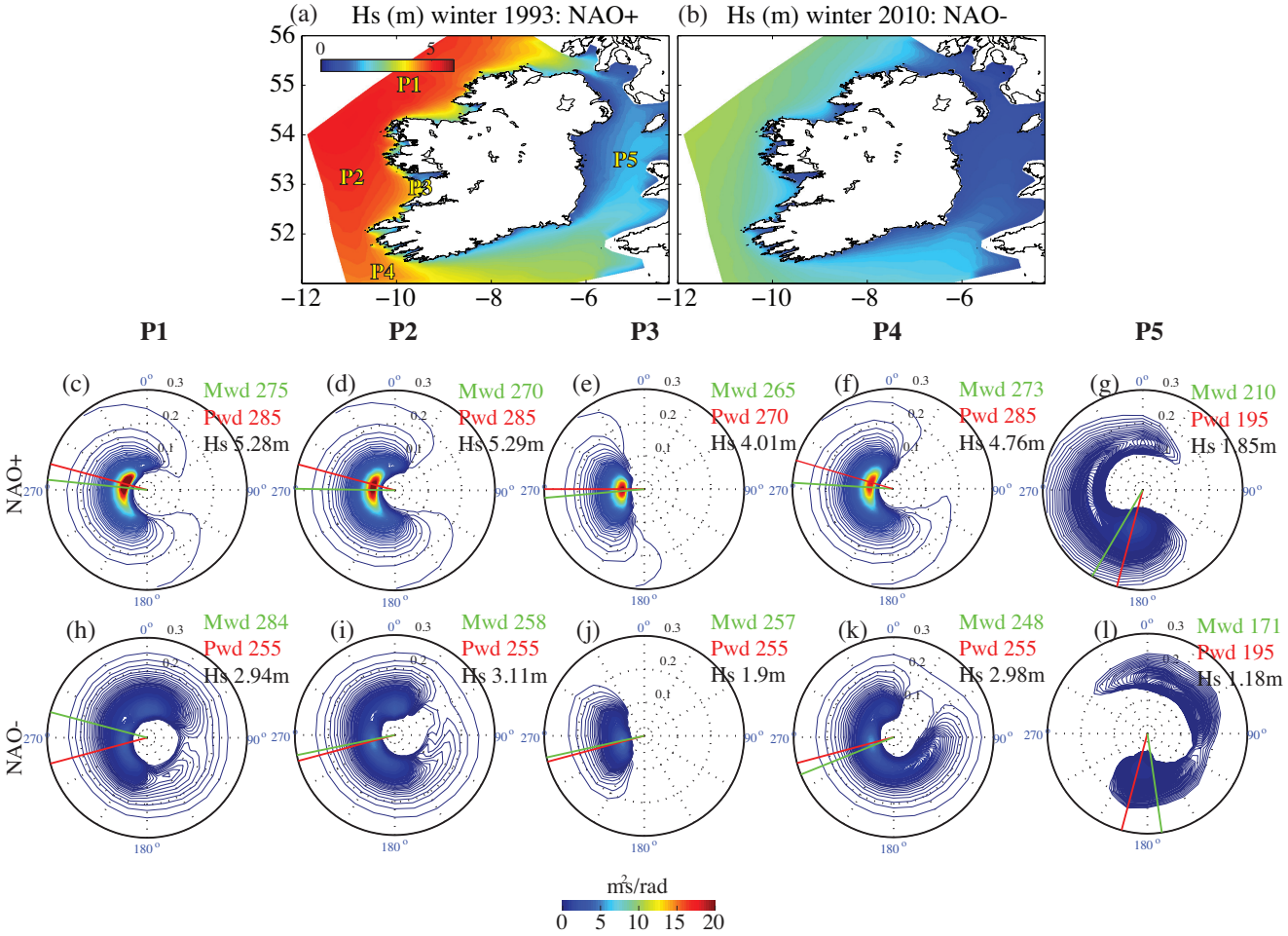

Fig. 17: Significant wave height for (a) winter 1993, corresponding to the maximum NAO winter index in the period 1979-2012 (depicted in Figure 16), (b) winter 2010, corresponding to minimum NAO winter index during 1979-2012. (c) - (g) Averaged wave-variance density spectra (m^2s/rad) for winter 1993 at the locations depicted in panel (a). For each point, the average significant wave height, mean wave direction (Mwd) and peak wave direction (Pwd) are displayed. (h)-(l) same as above, for winter 2010. *(Directions are given in the meteorological convention: 0° corresponds to waves coming from North, 90° corresponds to waves coming from East.)*

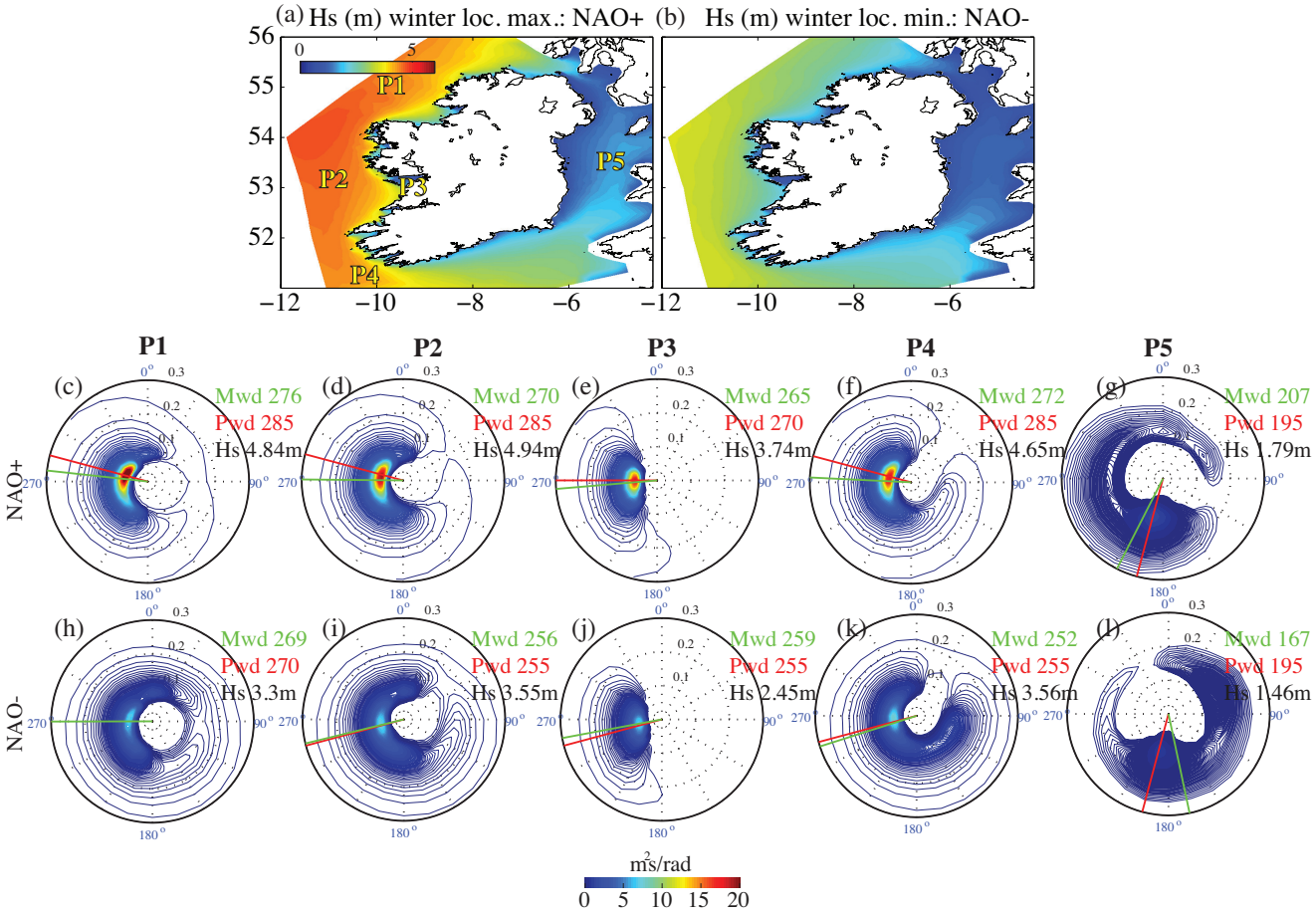

Fig. 18: Same as Figure 17, taking into consideration years with local maxima and minima respectively of the NAO winter index depicted in Figure 16.

of Figure 17) are staggering, in particular on the west coast, where decreases of more than 30% can be seen. The contrast is only slightly diminished when wave heights averaged over years with extreme NAO positive phases and negative phases respectively are considered (see panels (a) and (b) of Figure 18). Noteworthy is also the enhanced directional spread for the offshore points on the west coast (P1, P2 and P4) associated with the negative NAO indexes, in particular for the point P1, located in the northwest.

Furthermore, in the Irish Sea (point P5) the wave-energy spectra exhibits a directional reversal between the NAO positive phase and negative phase respectively (see panels (g), (l) of Figures 17 and 18 respectively). Indeed, negative phases of the NAO index generally give rise to a weakening of mid-latitude westerly winds with more occurrences of easterly winds in this region (Castro-Díez et al, 2002; Wilby et al, 1997). Interestingly, the point P3 located nearshore (at a depth of 60m), exhibits smaller directional spread during negative NAO phases as opposed to positive NAO phases, presumably due to the sheltering effects of the Aran islands which limits the fetch of the easterly winds. Finally, a northerly shift in both mean and peak direction associated with positive NAO phases can be seen at all points around the coast.

5 Summary and conclusions

A 34 year, high-resolution, nearshore wave hindcast was performed for Ireland, including both the Atlantic and the Irish Sea coasts. The model was validated with observations from 17 wave buoys around Ireland and with altimeter data from the CERSAT database. The comparison between the observations and the model was found to be excellent.

Strong seasonal, interannual and spatial variability was found for the significant wave height and the wave energy flux. We have also identified a strong correlation between the NAO teleconnection pattern and wave heights, wave periods and peak direction in winter and, to a lesser extent, in spring. The large variation in mean wave heights was found between strong values of winter NAO positive and winter NAO negative phases. A significant correlation with the EA teleconnection pattern was identified in autumn.

Acknowledgements This study was funded by Science Foundation Ireland (SFI) under the research project "High-end computational modelling for wave energy systems" and by the Sustainable Energy Authority of Ireland (SEAI) through the Renewable Energy Research Development & Demonstration Programme. The ESB, Met Éireann, the Marine Institute and Shell provided the buoy data for validation. The INFOMAR bathymetric datasets were provided by the Geological Survey Ireland (GSI) and the Marine Institute. The VORF software for tidal datum conversions was obtained from the GSI. The UKHO bathymetry was provided by OceanWise Ltd. The altimeter-derived wave data was obtained from the Centre de Recherche et d'Exploitation Satellitaire (CERSAT), at Ifremer, Plouzané, France in the frame of the Globwave project, funded by the European Space Agency (ESA). The authors thank Dr. C. Sweeney and Prof. P. Lynch (UCD School of Mathematical Sciences) for very helpful discussions, Dr. F. Ardhuin (Ifremer) for his advice regarding the WAVEWATCH code, M. Béchereau and P. Sweeney for their help with the construction of the DEM. Finally, the numerical simulations were performed on the Stokes cluster at the Irish Centre for High-end Computing (ICHEC) and at the Swiss National Computing Centre under the PRACE DECI 10 project "Nearshore wave climate analysis of the west coast of Ireland".

References

Appendini C, Camacho V (2012) Using GlobWave L2P data for wave hindcast assessments in the Gulf of Mexico. URL http://www.globwave.org/Tools/Case-Studies-Tutorials/Using-GlobWave-L2P-data-for-wave-hindcast-assessments-in-the-Gulf-of-Mexico/

Ardhuin F, Rogers E, Babanin A, Filipot JF, Magne R, Roland A, van der Westhuysen A, Queffeulou P, Lefevre JM, Aouf L, Collard F (2010) Semi-empirical dissipation source functions for wind-wave models: part I, definition, calibration and validation. J of Phys Oceanogr 40(9):1917–1941

Bacon S, Carter D (1993) A connection between mean wave height and atmospheric pressure gradient in the North Atlantic. Int J of Climatol 13:423–436

Barnston A, Livezey E (1987) Classification, seasonality and persistence of low-frequency atmospheric circulation patterns. Mon Weather Rev 115:1083–1126

Berens P (2009) CircStat: a MATLAB toolbox for circular statistics. J of Statistical Softw 31(10)

Bertin X, Prouteau E, Letetrel C (2013) A significant increase in waveheight in the North Atlantic Ocean over the 29th century. Glob and Planet Chang 106:77–83

Boudière E, Maisiondieu C, Ardhuin F, Accensi M, Pineau-Guillou L, Lespesqueue J (2013) A suitable metocean hindcast database for the design of marine energy converters. In: Proceedings of the 10th European Wave and Tidal Energy Conference Series EWTEC, Aalborg, Denmark

Cahill B, Lewis A (2011) Long term wave energy resource characterization of the Atlantic Marine Energy Test Site. In: Proceedings of the 9th European Wave and Tidal Energy Conference, Southampton, U.K.

Calder B (2006) On the uncertainty of archive hydrographic data sets. IEEE J of Ocean Eng 31(2):249–265

Castro-Díez Y, Pozo-Váquez D, Rodrigo F, Esteban-Parra M (2002) NAO and winter temperature variability in southern Europe. Geophys Res Lett 29(8):1–4

CERSAT (2013) Centre de Recherche et d'Exploitation Satellitaire (CERSAT). URL http://cersat.ifremer.fr/

Charles E, Idier D, Thiébot J, Le Cozannet G, Pedreros R, Ardhuin F, Planton S (2012) Present wave climate in the Bay if Biscay: Spatiotemporal variability and trends from 1958 to 2001. J of Clim 25(6):2020–2039

COASTALT (2014) The COASTALT Project. URL http://www.coastalt.eu/

Curé M (2011) A fifteen year model based wave climatology of Belmullet, Ireland. Tech. rep., A report prepared on behalf of the Sustainable Energy Authority of Ireland (SEAI).

Dee DP, Uppala SM, Simmons AJ, Berrisford P, Poli P, Kobayashi S, Andrae U, Balmaseda MA, Balsamo G, Bauer P, Bechtold P, Beljaars ACM, van de Berg L, Bidlot J, Bormann N, Delsol C, Dragani R, Fuentes M, Geer AJ, Haimberger L, Healy SB, Hersbach H, Hólm EV, Isaksen L, Kållberg P, Köhler M, Matricardi M, McNally AP, Monge-Sanz BM, Morcrette JJ, Park BK, Peubey C, de Rosnay P, Tavolato C, Thépaut, J-N, Vitart F (2011) The era-interim reanalysis: configuration and performance of the data assimilation system. Q J of the R Meteorol Soc 137(656):533–597

Dias F, Gallagher S, Gleeson E, McGrath R, Tiron R, Whelan E (2013) Spatial and seasonal variability of the nearshore wave and wind climate of Ireland:a high resolution hindcast for 2000-2012 with applications to the remewable energy sector. Tech. rep., Sustainable Energy Authority of Ireland

Dodet G, Bertin X, Taborda R (2010) Wave climate variability in the North-East Atlantic Ocean over the last six decades. Ocean Modelling 31:120–131

Dorschel B, Wheeler A, Monteys X, Verbruggen K (2011) Atlas of the Deep-Water seabed: Ireland. Springer

EMODnet (2013) EMODnet. http://www.emodnet-hydrography.eu/content/content.asp?menu

ESB (2005) Accessible wave energy resource atlas of Ireland. Tech. Rep. Report 4D404A-R2 for the Marine Institute and Sustainable Energy Ireland, ESB International

Folley M, Whitthaker T (2009) Analysis of the nearshore wave energy resource. Renew Energy 34:1709–1715

Gallagher S, Tiron R, Dias F (2013) A detailed investigation of the nearshore wave climate and the nearshore wave energy resource on the west coast of Ireland. In: Proceedings of the ASME 2013 32nd International Conference on Ocean, Offshore and Arctic Engineering OMAE, Nantes, France

GlobWave (2013) GlobWave project. URL http://www.globwave.org/

INFOMAR (2006) Integrated Mapping for The Sustainable Development of Ireland's Marine Resource (INFOMAR): A Successor to the Irish National Seabed Survey. Proposal & strategy. Dublin, Ireland

Janssen PAEM (2008) Progress in ocean wave forecasting. J of Computational Phys 227:3752–3594

LANDSAT (2013) Global mosaic of Landsat7. courtesy nasa/jpl-caltech. URL http://ows.geogrid.org/basemap

Le Cozannet G, Lecacheux S, Delvallee E, Desramaut N, C O, Pedreros R (2010) Teleconnection Pattern Influence on Sea-Wave Climate in the Bay of Biscay. J of Clim 24:641–652

Liberti L, Carillo A, Sannino G (2013) Wave energy resource assesment in the Mediterranean, the Italian perspective. Renew Energy 50:938–949

MI (2013) Irish Marine Weather Buoy Network. URL http://www.marine.ie/home/publicationsdata/data/buoys/

Climate Prediction Center NOAA (2013) NAO index. http://www.cpc.ncep.noaa.gov/data/teledoc/telecontents.shtm

Persson A (2011) User guide to ECMWF forecast products. Tech. rep., European Centre for Medium-Range Weather Forecasts (ECMWF), Shinfield Park, Reading, RG2 9AX, UK

Poti M, Kinlan B, Menza C (2012) A biogeographic assessment of sea birds, deep sea corals and ocean habitats of the New York bight: science to support offshore spatial planning., NOAA National Center for Coastal Ocean Science, chap 2

Queffeulou P, Croizé-Fillon D (2013) Global altimeter SWH data set. Tech. Rep. 10, Ifremer, Brest

Rascle N, Ardhuin F (2013) A global wave parameter database for geophysical applications. part 2: Model validation with improved source term parameterization. Ocean Modelling 70(0):174–188

Roland A (2008) Development of WWM II: Spectral wave modelling on unstructured meshes. PhD thesis, Institute of Hydraulics and Wave Resource Engineering, Technical University Darmstadt, Germany

Rute Bento A, Marinho P, Campos R, Guedes Soares C (2012) Modelling wave energy resources in the Irish West Coast. In: Proceedings of the 30th International Conference on Ocean, Offshore and Artic Engineering OMAE, Rotherdam, Netherlands

Taylor KE (2001) Summarizing multiple aspects of model performance in a single diagram. J Geophys Res 106(D7):7183–7192

Tiron R, Gallagher S, Dias F (2013) The influence of coastal morphology on the wave climate and wave energy resource of the West Irish Coast. In: Proceedings of the 10th European Wave and Tidal Energy Conference Series EWTEC, Aalborg, Denmark

Tolman H (2009) User manual and system documentation of Wavewatch III version 3.14. Tech. Rep. 276, NOOA/NWS/NCEP/MMAB

Wang X, Swail V (2001) Changes of extreme wave heights in Northern Hemisphere oceans and related atmospheric circulation regimes. J of Clim 14:2204–2221

Wang X, Swail V (2002) Trends of Atlantic wave extremes as simulated in a 40-year wave hindcast using kinematically reanalysed wind fields. J of Clim 15:1020–1035

Wessel P, Smith W (1996) A global self-consistent, hierarchical, high-resolution shoreline database. J of Geophys Res 101(B4):8741–8743

van der Westhuysen A (2012) Modeling nearshore wave processes. In: ECWMF Workshop on "Ocean Waves", European Centre for Medium-Range Weather Forecasts, Reading

WestWave (2013) ESB WestWave project. URL http://www.westwave.ie/

Wilby R, O'Hare G, Barnsley N (1997) The North Atlantic Oscillation and British Isles climate variability, 1865-1996. Weather 52(9):266–276